Ex vivo computed tomography evaluation of loading position on morphometry of the caudal cervical intervertebral disk spaces of dogs

Sebastian C. Knell Dr Med Vet
Lucas A. Smolders DVM, PhD
Thomas Steffen MD
Antonio Pozzi DVM, MS

Received January 31, 2018.
Accepted July 30, 2018.

From the Clinic for Small Animal Surgery (Knell, Smolders, Pozzi) and Musculoskeletal Research Unit (Steffen), Vetsuisse Faculty, University of Zurich, 8057 Zurich, Switzerland; and Orthopaedic Research Laboratory, Division of Orthopaedic Surgery, McGill University, Montreal, QC H3G 1A4, Canada (Steffen).

Address correspondence to Dr. Knell (sknell@vetclinics.uzh.ch).

OBJECTIVE
To provide an objective, quantitative morphometric description of the caudal cervical intervertebral disk (IVD) spaces of dogs.

SAMPLE
Vertebral specimens consisting of C4 through C7 from 5 medium-sized dogs.

PROCEDURES
CT images were obtained with the specimens positioned in neutral, flexion, extension, and lateral bending positions. Size and shape of the cranial and caudal end plates, angle between the end plates (IVD wedge angle), and craniocaudal distance (IVD width) between end plates for the 4 loading positions were measured and compared for the 3 segments (C4-5, C5-6, and C6-7).

RESULTS
End plate size and shape, IVD wedge angle, and IVD width were not significantly different among the 3 segments. Caudal cervical end plates were consistently larger than cranial cervical end plates. The IVD wedge angle ranged from −4.8° to 15.2°. Flexion induced a reduction in IVD width in the ventral portion of the IVD, whereas extension induced a decrease in width in the dorsal portion of the IVD. Central IVD width remained unchanged among the loading positions.

CONCLUSIONS AND CLINICAL RELEVANCE
Unique morphometric and dynamic characteristics of the caudal cervical IVD space of dogs were detected. These findings may help investigators when designing IVD prostheses for dogs with cervical spondylomyelopathy. (*Am J Vet Res* 2019;80:235–245)

Caudal cervical spondylomyelopathy is a common disease of the cervical vertebrae in large-breed dogs that leads to various neurologic clinical signs caused by static and dynamic compression of the spinal cord.[1,2] Most of the so-called disk-associated CSMs involve IVD degeneration and prolapse between C5 and C6 and between C6 and C7.[2] The pathogenesis, diagnosis, and treatment of this disease are controversial, largely because the disease is not completely understood.

Treatment for CSM can be medical or surgical.[2] Surgical treatment has a better overall outcome and therefore is recommended in most cases.[3] Surgical treatment may consist of direct decompression (eg, partial removal of a bulging IVD via a ventral approach) or indirect decompressive techniques (eg, distraction and fusion of the affected vertebral segment[2,4]). However, decompressive techniques often lead to delayed fusion of the involved segments.[5] Although these surgical techniques are generally satisfactory, it has been suggested that they can promote a change in vertebral kinematics and consequently a shift of the disease toward adjacent segments (adjacent segment disease) in up to 20% of the cases.[6] Canine patients are often euthanized when there is recurrence of clinical signs originating from an adjacent segment.[4]

With the aim of preserving vertebral kinematics after surgical intervention, there has been an increasing interest in the development of new surgical techniques for canine patients with CSM. One of these techniques involves inserting an artificial IVD into the IVD space, with the goal of reestablishing normal vertebral motion.[7,a] However, this technique is associated with various complications, including delayed bone ingrowth, subsidence of the implant at the bone interface, lack of osseointegration, and incomplete restoration of vertebral kinematics.[8,b] Such complications may arise from a mismatch between the shape of current prosthesis designs and the rather asymmetric and obliquely orientated cervical IVD space. This discrepancy between anatomy and implant design

ABBREVIATIONS

CSM	Caudal cervical spondylomyelopathy
IVD	Intervertebral disk

may result in abnormal loading between the prosthesis and adjacent end plates. When considering potential improvements to current prosthesis designs, an anatomically shaped prosthesis conforming to the natural shape and size of an IVD space in dogs can be expected to more closely match the dynamic properties of the disk space. However, to our knowledge, a blueprint for such a prosthesis (ie, a fundamental morphometric description of the canine caudal cervical IVD space in a neutral position and in various loading positions) has not been described.

The aims of the study reported here were to determine the shape and size of the cranial and caudal end plates of the canine C4-5, C5-6, and C6-7 IVD spaces and to calculate the intervertebral angles and dimensions (IVD width) of the C4-5, C5-6, and C6-7 spaces in neutral, flexion, extension, and lateral bending positions. We hypothesized that the size and shape of the cranial end plate would differ from those of the caudal end plate, IVD wedge angles and width would change significantly throughout the physiologic range of motion, and morphometric characteristics would not differ among the C4-5, C5-6, and C6-7 spaces.

Materials and Methods

Sample

Vertebral specimens (C4 through C7) were harvested from cadavers of 5 skeletally mature mixed-breed dogs that were euthanized for reasons unrelated to the study. Owners provided written consent to use the cadavers for research purposes. Body weight ranged from 25 to 35 kg. Radiography was performed to rule out pathological changes. Muscular attachments were removed, but ligaments and IVDs were left intact. Specimens were stored at –18°C in towels soaked in saline (0.9% NaCl) solution to prevent dehydration. Specimens were thawed at 4° to 8°C during a 24-hour period before testing.

Specimen preparation

Two Steinmann pins (4.0 mm in diameter) were inserted into the vertebral bodies of both C4 and C7 to allow biomechanical loading of the specimens. One pin was oriented in the transverse plane perpendicular to the vertebral column and pointing in a laterolateral direction, whereas the other pin was oriented in the sagittal plane in a dorsoventral direction. Metallic beads were inserted in the spinous processes of C4 through C7 for alignment purposes. Beads were positioned in the midsagittal plane at two-thirds the dorsoventral height at the caudal end of each spinous process.

Specimens were mounted on a custom-made loading jig with 2 fixed polyvinylchloride blocks (1 on each side) so that the vertebrae were mounted between the blocks **(Figure 1)**. These blocks had a 4-mm hole on one end and a slot on the other end, which spanned almost the entire block. The laterolateral Steinmann pin positioned in C7 was inserted into the slot, which allowed the specimen to slide when torque was applied. In contrast, the laterolateral Steinmann pin positioned in C4 was placed through the hole in the polyvinylchloride block, which thereby provided a point of fixation.

Load application

Specimens were mounted in the loading jig, and the cranial vertebral segment was fixed in position. A targeted torque of 1.5 N•m (magnitude chosen on the basis of an ex vivo study[9] of dogs) was applied to the pins (laterolateral and ventrodorsal) anchored in the caudal segment of a vertebral specimen. Torque was applied by use of a handheld loading scale that displayed the number of kilograms. The cranial vertebral segment was fixed in the jig by means of the 2 pins, which thereby allowed vertebral motion only at the caudal end of a specimen. Each specimen was loaded in flexion, extension, and lateral bending. For flexion and extension, torque was applied to the ventrodorsal pin in C7 from the dorsal or ventral side of the vertebra, respectively. We assumed that right and left lateral bending were identical; therefore, only left lateral bending was induced by applying torque on the left lateral pin. After torque was applied, the specimen was fixed in loading positions by use of an external skeletal fixator.[c] The loaded vertebral specimen was then scanned in this fixed position, which allowed standardized measurement of the cervical IVD spaces.

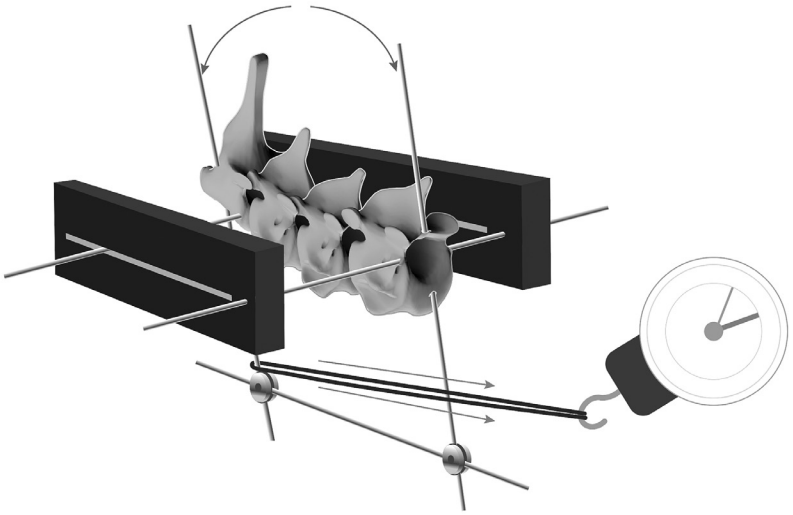

Figure 1—Schematic illustration of the experimental setup for canine cervical specimens consisting of segments C4 through C7. The cranial end of the specimen is toward the scale. Two orthogonal 4.0-mm-diameter Steinman pins were inserted in the transverse and sagittal plane of C4 and C7. An external skeletal fixator was mounted to maintain various loading positions (neutral, flexion, extension, and lateral bending). Pins in the cranial segment were fixed in a hole in each polyvinylchloride bar, whereas pins in the caudal segment were placed through a slot to direct the applied torque to 1 direction.

CT imaging

Computed tomographic images[d] were obtained of each specimen in neutral, flexion, extension, and lateral bending positions. Scanning was performed at 120 kV and 250 mA, with a pitch of 0.688, rotation time of 0.75 seconds, and detector collimation of 16 X 0.75. Raw data were reconstructed in a bone algorithm with an increment of 0.5 mm. Images were exported to a workstation for data analysis with a DICOM viewer.[e]

To achieve consistent measurements of IVD width, predetermined reference points were defined on the cranial and caudal end plates of C4 through C7. First, images were aligned in a repeatable manner for each specimen, segment, and loading position in the sagittal, dorsal, and transverse planes to enable standardized identification of orientation points. Alignment was performed by use of specific landmarks on 3-D multiplanar CT reconstruction images.

To achieve alignment in the sagittal plane, metal beads placed in the spinal processes were aligned **(Figure 2)**. To achieve alignment in the dorsal plane, transverse reconstruction images were used. A line was drawn that intersected the transverse processes immediately ventral to the transverse foraminas in the cranial segment. To achieve alignment in the transverse plane, the midsagittal reconstruction was used. First, the IVD wedge angle was measured on the midsagittal plane of the IVD space by use of the sagitally reconstructed CT images. Bony protrusions surrounding the region of the nucleus pulposus of both cranial and caudal end plates were identified. A line connecting these landmarks was drawn for each end plate (defined as lines ECd and ECr for the caudal and cranial end plate, respectively). A line was then drawn to bisect the IVD wedge angle between the cranial and caudal end plate (defined as line Bis); this line was used for alignment of the transverse plane. When the cranial and caudal end plate orientation lines (ie, lines ECd and ECr) were parallel, the midline between these 2 orientation lines was referenced as a bisector line.

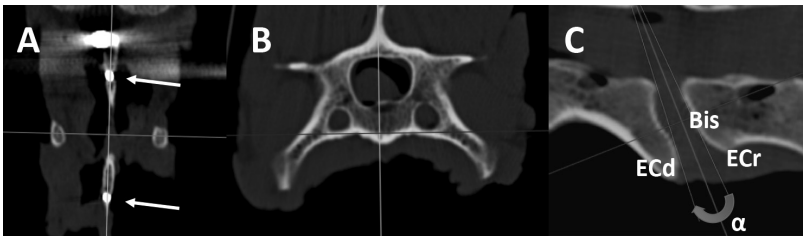

Figure 2—Computed tomographic images illustrating multiplanar reconstruction for alignment of vertebral specimens in the dorsal (A), transverse (B), and sagittal (C) planes. A—Alignment in the sagittal plane (vertical orientation line) was achieved by use of the dorsal reconstruction and aligning beads (arrows) that were inserted in the spinal processes. B—Alignment of the dorsal plane was achieved by use of the transverse reconstruction and drawing a line through the base of the transverse processes ventral to the transverse foramen. C—Alignment in the transverse plane was achieved by use of the sagittal reconstruction and drawing orientation lines that intersected the prominent surface points on the cranial and caudal end plates (ECr and ECd, respectively) in the area of the nucleus pulposus; these lines were used to define the IVD wedge angle (α) between the end plates. The middle line (Bis) represents the line that bisects the IVD wedge angle.

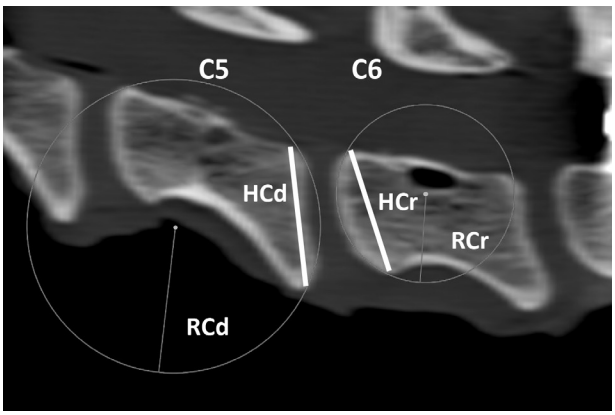

Figure 3—Sagittal CT image of a vertebral specimen indicating measurements of static variables of the end plates. End plate curvature was measured by matching the shape of the cranial and caudal end plates to a circle. Radius of the cranial end plate (RCr) and caudal end plate (RCd) was then measured. Height of the end plates was measured on the cranial (HCr) and caudal (HCd) end plates as the distance from the most dorsal to the most ventral bony landmark of the end plates. Notice that the cranial and caudal end plates are in relation to a particular vertebra and not in relation to the IVD space.

Morphometric variables

Measurements were obtained from the reconstructed CT images by 1 investigator (SCK). A second investigator (LAS) and the aforementioned investigator (SCK) measured a subset of end plate distances to confirm consistent intraobserver and interobserver measurements. Variables were defined as static or dynamic. Static variables were defined as measurements that were not changed by vertebral motion, whereas dynamic variables were defined as measurements that changed throughout vertebral motion.

Static variables—Static variables were measured for the cranial and caudal end plates of the IVD spaces for each of the 3 segments (C4-5, C5-6, and C6-7). Reference to a cranial or caudal end plate was made with respect to the cranial and caudal aspect of a particular vertebra and not in relation to the IVD space (eg, the cranial end plate for the C4-5 space was the cranial end plate of the vertebral body of C5, and the caudal end plate was the caudal end plate of the vertebral body of C4). Static variables included end plate height and width as well as end plate morphology. End plate height was defined as the maximum distance from the dorsal to the ventral tip of the end plate as measured in the midsagittal plane for the cranial and caudal end plate, respectively **(Figure 3)**. End plate width was defined as the left-to-right margin of the end plate in the middorsal plane.

End plate morphology was described for all sagittal reconstructed planes on the basis of shape[10] and radius of the curvature. Shape of the cranial and caudal end plates on the sagitally reconstructed CT images was categorized on the basis of a previously published[10] end plate morphology system that involved the use of radiography **(Figure 4)**. In the present study, sagittal CT images were categorized on the basis of the shape of the end plate as 1 of 3 types: concave when the center of the end plate was lower than the peripheral portion of the end plate, flat when the center of the end plate and the peripheral portion of the end plate were in the same plane without any curvature, and convex when the center of the end plate was ≥ 1 mm higher than the peripheral portion of the end plate. Furthermore, when an end plate was categorized as convex, the curvature apex was further classified as a single apex when there was only 1 apex or a double apex when there were 2 apices with a concavity in between.

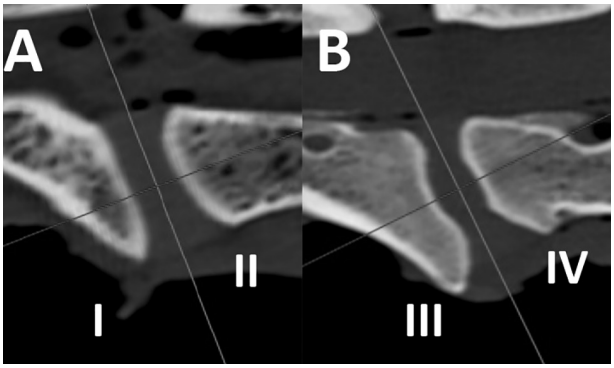

Figure 4—Dorsal CT images of a C5-C6 segment obtained through predefined planes a (A) and c (B). Five equidistant lines were created from the cranial to the caudal end plate parallel to the long axis of the vertebrae from the right lateral to the left lateral border of the caudal end plate (lines were labeled a through e from left to right to define 5 sagittal plane images). For both images, cranial is to the left. A—In the laterolateral periphery of plane a, the caudal end plate of the cranial vertebral body has a flat surface (I), whereas the cranial end plate of the caudal segment has a convex shape with a single apex (II). B—Both end plates are convex, but the caudal end plate of the cranial segment has double apices (III), whereas the cranial end plate of the caudal segment has only 1 apex (IV). Within the 2 apices for the cranial end plate of the caudal segment (IV), the shape appears to be concave; however, we considered the overall shape of the end plate to be convex.

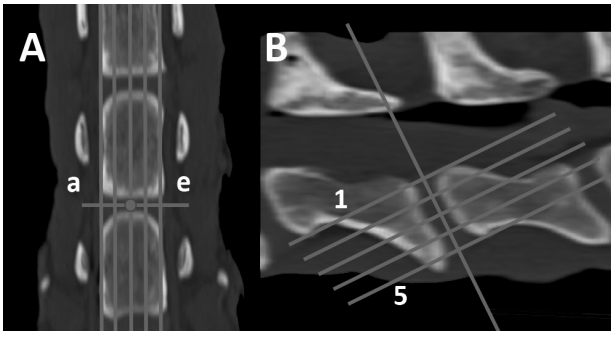

Figure 5—Dorsal (A) and sagittal (B) CT images of a vertebral specimen. A—The image is at the level of the dorsal tip of the caudal end plate. Lines a through e are equidistant and parallel and divide the IVD space into 5 sagittal planes. Line c is indicated (gray circle). B—Sagittal view corresponding to line c. Five lines (labeled 1 through 5 from dorsal to ventral) were drawn. Measurement of the IVD width was determined for these lines, which were oriented perpendicular to the bisector line through the IVD space.

End plate curvature was measured by matching a circle to the shape of the cranial and caudal end plates (Figure 3). Radius of the matching circle was used as a measure of end plate curvature. In case of a concave shape, the radius of the end plate was expressed as a negative value, whereas a convex shape was reported as a positive value.

Dynamic variables—Dynamic variables included IVD wedge angle and IVD width for various loading positions and were measured for all 3 segments for each of the 4 loading positions **(Figure 5)**. Landmarks for measurement of IVD wedge angle were described in detail previously for the alignment in the transverse plane.

The angle between the 2 lines that intersected the end plate (lines ECd and ECr for the cau-

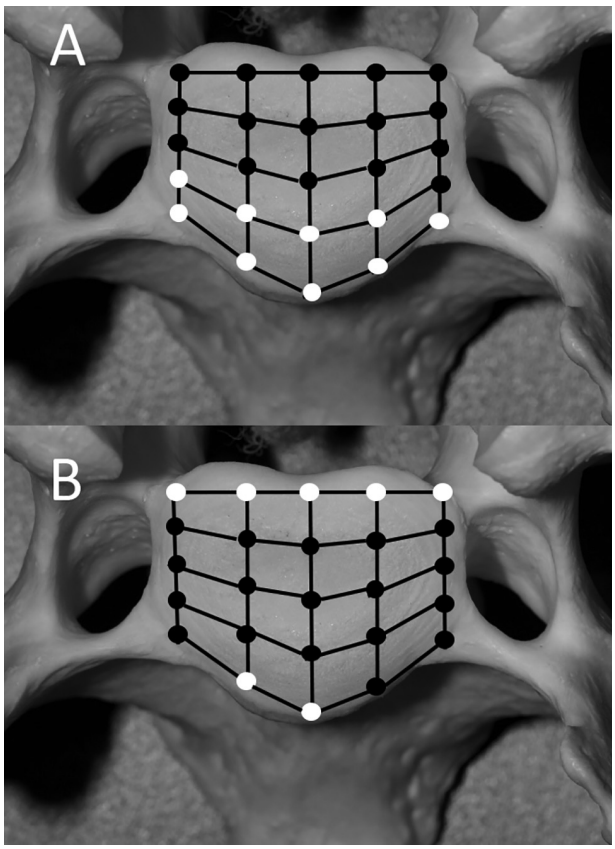

Figure 6—Schematic illustration of 25 predefined landmarks on the cranial bony end plate of a vertebral specimen in flexion (A) and extension (B). Locations that have significant ($P < 0.05$) changes for IVD measurements, compared with values for the neutral position, are indicated as white circles, whereas locations with nonsignificant changes are indicated as black circles. Notice the irregular distribution of the grid.

dal and cranial end plate, respectively; Figure 2) was defined as the IVD wedge angle α. When these lines were parallel, the angle was recorded as 0°. A positive value indicated that the angle opened ventrally, whereas a negative value indicated that the angle opened dorsally.

The IVD width was defined as the distance between the cranial and caudal end plates on the sagittal image. Because there were not 25 specific anatomic locations on the end plate and we wanted to obtain an objective description of IVD width of individual disk spaces, the distance between the cranial and caudal end plates was measured at 25 locations over the end plates. To create this grid, the first step was to define a dorsal plane at the dorsal tip of the end plate of each segment in the multiplanar CT reconstruction. In this dorsal plane, 5 equidistant lines were created from the cranial to the caudal end plate parallel to the long axis of the vertebrae from the right lateral to the left lateral border of the caudal end plate (lines were labeled a through e from left to right to define 5 sagittal planes; Figure 5). Each sagittal plane image was exported to enable us to obtain measurements.

The IVD width was measured perpendicular to the intervertebral bisection (line Bis; Figure 2) at 5 locations and defined separately for each of the 5

Table 1—Mean ± SD end plate height, end plate width, and curvature (radius) of vertebral segments for specimens obtained from 5 canine cadavers.

Variable	End plate*	C4-5	C5-6	C6-7	Overall
Height (mm)	Cranial	13.7 ± 1.7	14.1 ± 0.8	15.0 ± 1.8	15.0 ± 1.2
	Caudal	17.0 ± 1.5	17.2 ± 1.2	16.5 ± 1.3	17.8 ± 2.0
Width (mm)	Cranial	15.7 ±1.3	15.0 ± 0.7	14.2 ± 1.8	14.0 ± 1.4
	Caudal	18.0 ± 2.4	17.0 ± 2.1	17.8 ± 1.9	17.0 ± 1.3
Curvature (mm)	Cranial	10.6 ± 2.3	9.9 ± 1.1	10.2 ± 3.4	10.2 ± 1.4
	Caudal	12.2 ± 3.7	13.5 ± 2.3	13.5 ± 4.6	13.5 ± 3.4

*Cranial and caudal endplates are in relation to a particular vertebra and not in relation to the IVD space (eg, for the C4-C5 segment, the caudal end plate is from C4 and the cranial end plate is from C5).

Table 2—Shape of the cranial and caudal end plates* at 5 sagittal planes (a through e) for vertebral segments obtained from 5 canine cadavers.

Sagittal plane	Shape	C4-5		C5-6		C6-7	
		Cranial	Caudal	Cranial	Caudal	Cranial	Caudal
a	Concave	0	0	0	0	0	0
	Flat	1	4	2	1	1	5
	Convex						
	Single apex	4	1	3	4	4	0
	Double apices	0	0	0	0	0	0
b	Concave	0	0	0	0	0	0
	Flat	0	0	0	0	0	0
	Convex						
	Single apex	5	0	5	0	5	0
	Double apices	0	5	0	5	0	5
c	Concave	0	0	0	0	0	0
	Flat	0	0	0	0	0	0
	Convex						
	Single apex	4	1	5	0	5	0
	Double apices	1	4	0	5	0	5
d	Concave	0	0	0	0	0	0
	Flat	0	0	0	0	0	0
	Convex						
	Single apex	5	0	5	0	5	0
	Double apices	0	5	0	5	0	5
e	Concave	0	0	0	0	0	0
	Flat	3	3	2	2	2	5
	Convex						
	Single apex	2	2	3	3	3	0
	Double apices	0	0	0	0	0	0

In the dorsal plane image, 5 equidistant lines were created from the cranial to the caudal endplate parallel to the long axis of the vertebrae from the right lateral to the left lateral border of the caudal endplate (lines were labeled a through e from left to right to define 5 sagittal planes). Shape was categorized as concave, flat, and convex as described elsewhere.[10] When an end plate was categorized as convex, the curvature apex was further classified as a single apex or double apices.

See Table 1 for remainder of key.

sagittal planes. Line 1 started at the craniodorsal tip of the cranial end plate of the caudal vertebral body. Similarly, line 5 was created by drawing a line from the most cranioventral tip of the cranial end plate of the caudal segment (Figure 5). Three additional lines were added between lines 1 and 5 such that the lines were equidistant. These 5 lines were labeled from 1 through 5 (dorsal to ventral). By use of lines 1 through 5, IVD width was measured at 5 dorsoventral levels for all sagittal slices (planes a through e), which resulted in a map of the IVD width at 25 locations **(Figure 6)**. However, because the height of the end plate differed among the sagittal planes (eg, the end plate height at sagittal plane a was smaller than the end plate height at sagittal plane c), the 25 points on the IVD map were not evenly distributed.

After testing was completed, all specimens were cut in half in the sagittal plane to enable identification of abnormal or degenerated disks, which were excluded. Degenerative state of the IVDs (C4-5, C5-6, and C6-7 spaces) was graded in accordance with the Thompson grading scale.[11] Specimens with a grade > 2 were excluded from the study.

Data analysis

For all variables with continuous data, mean ± SD were calculated separately for the C4-5, C5-6, and C6-7 IVD spaces. Changes in IVD width were also expressed as a percentage of the distance from the neutral position.

Inferential statistics were performed with commercial software.[f] Linear mixed models were created to compare static variables between end plates (cranial and caudal), among segments (C4-5, C5-6, and C6-7), and among dynamic variables for the 4 loading positions (neutral, flexion, extension, and lateral bending) and segments. The Akaike information criterion was used for model selection. Normal distribution of the response variables within each model was assessed with PP and QQ plots. End plate morphology measurements were compared for shape (proportion with a specific shape) among the segments and between the cranial and caudal end plate by use of a Fisher exact test. The Benjamini-Hochberg correction was used to correct for multiple comparisons. Significance was set at $P < 0.05$.

To validate whether various measurements were comparable between observers and repeatable for the same observer, IVD width measurements (100 measurements for 4 specimens in neutral position) were compared for the same observer (SCK) and for 2 observers (SCK and LAS). Bland-Altman analysis was used to estimate mean bias, SD, and 95% limits of agreement (mean bias ± 1.96•SD). Furthermore, significance of intraobserver and interobserver measurements were compared by use of a Mann-Whitney test.[g] Significance was set at $P < 0.05$.

Results

Specimens and torque application

The C4-5, C5-6, and C6-7 IVDs of all vertebrae were scored as Thompson grade 1, except for the C6-7 IVD of 1 specimen, which was scored grade 2. Therefore, all disk spaces were included in the data analysis.

The angle of the applied force in relation to the specimen and the lever arm of the applied force were measured to evaluate whether the desired torque of 1.5 N•m was applied to each specimen. Mean ± SD actual torque was 1.9 ± 0.3 N•m for flexion and lateral bending and 2.1 ± 0.3 N•m for extension.

Static variables

Mean ± SD overall height and width of the cranial end plate were 15.0 ± 1.2 mm and 14.0 ± 1.4 mm, respectively **(Table 1)**. Mean height and width of the caudal end plate were 17.8 ± 2.0 mm and 17.0 ± 1.3 mm, respectively. Height and width of the caudal end plate were significantly ($P < 0.001$) greater than values for the cranial end plate for all segments. No significant ($P = 0.544$) differences were found between C4 and C5, C5 and C6, and C6 and C7.

Regarding end plate morphology, the cranial and caudal end plates were always categorized as straight or convex **(Table 2)**. There was a significant ($P < 0.001$) difference between the cranial and caudal end plate shape (single apex or double apices, respectively). When only the central planes (planes b through d) were evaluated, the end plate was always convex with a single apex or double apices. There was no significant ($P = 1.000$) difference among the 3 segments. Mean ± SD radius of the caudal end plates (13.5 ± 3.4 mm) was significantly ($P < 0.001$) larger than the radius of the cranial end plates (10.2 ± 1.4 mm; Table 1). Values did not differ significantly ($P = 0.544$) among segments.

Dynamic variables

Mean ± SD overall IVD wedge angle in the neutral position was 5.0 ± 2.6° **(Table 3)**. The IVD wedge angles did not differ significantly ($P = 0.734$) among

Table 3—Mean ± SD IVD wedge angle of vertebral segments for specimens obtained from 5 canine cadavers and measured in each loading condition.

Variable	IVD space	Neutral	Flexion	Extension	Lateral bending
Angle (°)	C4-5	5.0 ± 3.0	–5.0 ± 2.1	16.0 ± 4.3	5.0 ± 3.8
	C5-6	5.6 ± 3.3	–4.0 ± 2.2	15.0 ± 7.6	6.2 ± 3.0
	C6-7	3.8 ± 2.9	–7.0 ± 4.5	12.9 ± 9.8	5.0 ± 7.6

Positive values indicate that the angle opened ventrally, whereas negative values indicate that the angle opened dorsally.

the 3 segments. Mean IVD wedge angle decreased significantly ($P < 0.001$) in flexion (–4.8 ± 2.1°) and increased significantly ($P < 0.001$) in extension (15.2 ± 4.3°). Mean IVD wedge angle did not change significantly in lateral bending **(Figure 7)**.

Intervertebral motion resulted in significant changes in IVD width **(Table 4)**. Flexion resulted in a significant ($P < 0.001$) decrease in width in the ventral aspect of the IVD space (9/25 [36%] measurements). Compared with results for the neutral position, extension resulted in a significant ($P < 0.001$) decrease in IVD width in the dorsal aspect of the IVD space (5/25 [20%] measurements), whereas IVD width increased only at 2 positions in the ventral aspect of the IVD space **(Table 5)**. The IVD width of the central aspect of the IVD space did not differ significantly (all $P > 0.200$) during all positions (11/25 [44%] measurements). These changes in IVD width did not differ significantly ($P = 0.538$) among all 3 segments. The IVD width did not change significantly in lateral bending.

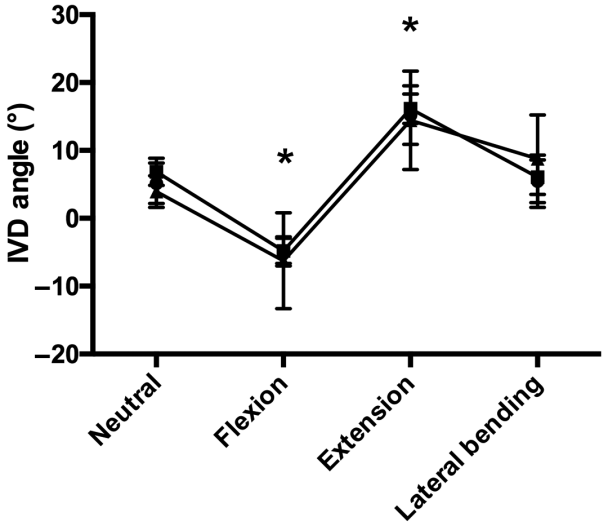

Figure 7—Mean ± SD values for IVD wedge angle for the segments C4-5 (circles), C5-6 (squares), and C6-7 (triangles) when the vertebrae were subjected to various loading conditions. Positive values indicate that the angle opened ventrally, whereas negative values indicate that the angle opened dorsally. *Value differs significantly ($P < 0.05$) from the values for all other loading conditions.

Intraobserver and interobserver agreement

Mean ± SD bias for intraobserver agreement was –0.18 ± 0.63 mm. The 95% limits of agreement were from –1.4 to 1.0 mm. The first measurements did not differ significantly ($P = 0.380$) from the second measurements.

Mean ± SD bias for interobserver agreement was –0.16 ± 0.77 mm. The 95% limits of agreement were from –1.7 to 1.4 mm. Measurements did not differ significantly ($P = 0.46$) between observers.

Discussion

The study reported here provided a morphological description of the caudal cervical IVD space and end plates of canine cadavers. The shape and size of the cranial and caudal end plates were clearly distinct from each other, which thereby confirmed our first hypothesis.

Table 4—Mean ± SD distance (mm) between landmarks on end plates of vertebral segments for specimens obtained from 5 canine cadavers and measured in each loading condition.

Loading condition	Line	Sagittal plane				
		a	b	c	d	e
Neutral	1	7.8 ± 1.1	6.9 ± 0.8	5.6 ± 0.4	6.3 ± 0.6	8.0 ± 1.0
	2	6.1 ± 0.6	4.5 ± 0.6	4.4 ± 0.7	4.0 ± 0.7	6.2 ± 0.8
	3	5.8 ± 0.7	4.5 ± 0.8	4.8 ± 0.8	4.3 ± 0.6	5.6 ± 0.7
	4	6.1 ± 0.6	4.9 ± 0.8	4.5 ± 0.6	4.1 ± 0.5	6.2 ± 0.6
	5	8.4 ± 1.0	8.2 ± 0.7	8.1 ± 0.6	8.4 ± 0.6	8.1 ± 0.5
Flexion	1	7.8 ± 1.3	6.3 ± 0.8	5.5 ± 0.8	6.4 ± 0.9	7.6 ± 0.8
	2	5.9 ± 0.8	4.4 ± 0.5	4.4 ± 0.7	4.6 ± 0.9	5.7 ± 0.7
	3	5.1 ± 1.5	4.1 ± 0.9	4.4 ± 0.7	4.2 ± 1.1	5.5 ± 0.8
	4	5.2 ± 1.4	3.5 ± 0.8	3.3 ± 0.9	3.6 ± 0.9	5.6 ± 0.7
	5	6.8 ± 1.3	6.5 ± 0.9	6.4 ± 1.0	6.1 ± 1.1	7.1 ± 1.2
Extension	1	6.4 ± 1.0	4.9 ± 0.7	4.5 ± 0.6	4.7 ± 0.7	6.8 ± 0.9
	2	4.9 ± 0.8	4.0 ± 0.7	3.9 ± 0.9	3.8 ± 0.7	5.3 ± 0.8
	3	5.1 ± 0.9	4.5 ± 0.8	4.9 ± 0.8	4.5 ± 0.8	5.5 ± 0.7
	4	6.2 ± 0.8	5.0 ± 0.8	4.9 ± 0.8	4.9 ± 0.9	6.1 ± 0.7
	5	8.1 ± 0.9	8.7 ± 1.4	9.6 ± 1.5	9.4 ± 1.7	7.8 ± 1.2
Lateral bending	1	7.0 ± 1.5	5.8 ± 1.0	5.0 ± 0.6	5.6 ± 1.2	7.6 ± 1.6
	2	5.5 ± 1.1	4.1 ± 0.8	4.2 ± 0.6	4.4 ± 0.8	6.0 ± 1.6
	3	5.5 ± 1.2	4.2 ± 1.3	4.6 ± 0.8	4.8 ± 1.0	5.8 ± 1.4
	4	5.8 ± 1.3	4.2 ± 1.0	4.2 ± 0.8	4.6 ± 0.8	6.6 ± 1.4
	5	6.7 ± 1.7	6.6 ± 1.3	8.1 ± 1.3	7.5 ± 1.4	7.8 ± 1.4

In the sagittal plane image, 5 equidistant lines were drawn, which created a grid from 1 (dorsal) to 5 (ventral).
See Table 2 for remainder of key.

Table 5—Mean percentage change for each of 25 predetermined IVD end plate locations in vertebral specimens obtained from 5 canine cadavers.

		Sagittal plane				
Change	**Line**	**a**	**b**	**c**	**d**	**e**
Flexion	1	–1	–5	–5	2	–5
	2	–4	–6	–1	3	–7
	3	–12	–12	–9	–10	–7
	4	–25*	–40*	–33*	–22*	–16
	5	–25*	–32*	–38*	–36*	–18*
Extension	1	–23*	–36*	–27*	–34*	–19*
	2	–26	–16	–14	–16	–15
	3	–18	–2	2	–2	–7
	4	–5	2	10	10	–7
	5	–5	7*	16*	10	–8

Values indicate the percentage change for each position, compared with results for the neutral position.
*Value differs significantly ($P < 0.05$) from the value for the neutral position.
See Tables 2 and 4 for remainder of key.

Significant changes in dynamic variables, IVD wedge angle, and IVD width among loading conditions confirmed our second hypothesis. The IVD wedge angle changed from a mean of 15.2° in extension to –4.8° in flexion, which indicated a total range of motion of approximately 20°. Moreover, the IVD width changed significantly during loading conditions, and different regions of the disk behaved differently, with the central region remaining largely unchanged, whereas the dorsal and ventral regions changed significantly in flexion and extension.

The aforementioned measures were found to be similar for the 3 segments tested; therefore, we accepted our third hypothesis. These findings indicated that a symmetric IVD prosthesis would be destined to mismatch the complex anatomy of cervical disk spaces and that a complex, asymmetric disk prosthesis may be required to accurately match the shape and size of the cranial and caudal end plates. However, the size and shape of the caudal cervical segments appeared to be similar.

Only limited data about the IVD width in dogs are currently available. In 2 reports,[12,13] IVD width (as measured with MRI in the middle of the end plate in dogs with and without clinical signs of CSM) ranged from 4.3 to 5.8 mm. The IVD width did not differ between the caudal cervical segments in 1 study.[13] In the present study, mean ± SD IVD width was 4.8 ± 0.8 mm in the middle of the IVD space. Although not completely comparable because of differences in methods (CT vs MRI), cohorts of dogs (mixed-breed dogs vs Doberman Pinschers), type of measurements (ex vivo vs in vivo), and methods to select the midpoint of the end plate, results of that study[13] and the present study can be largely regarded as similar.

Except for central IVD width, other morphometric variables of the caudal cervical disk space in dogs have not been reported to our knowledge. Studies have been conducted to evaluate the motion pattern of the human vertebral column and to compare the vertebral anatomy between humans and domestic animals.[14–16] However, morphology of the IVD space has not been compared between humans and dogs. When results of the present study were compared with data from the human literature, several similarities and differences were noted. With respect to absolute size, the end plate of humans is slightly wider (18 ± 4.8 mm) but of similar height (16.6 ± 1.8 mm) to the end plate of dogs. In contrast to results for dogs, the cranial end plate (ie, superior end plate) of humans is larger than the caudal (ie, inferior) end plate.

In contrast to end plate size, there are obvious differences between the shape of the cervical end plates of humans and dogs. Typically, the cranial end plate of humans is flat, whereas the caudal end plate is concave.[17] However, as was reported in the present study, the cranial and caudal end plates of dogs have a convex shape. In addition, a difference between the cranial and caudal end plates of dogs was found in that an end plate could have a single apex or double apices, shapes that have also been described in the lumbar vertebral column of humans.[10]

Several studies[10,18–21] have been conducted to investigate the human IVD space in a neutral position. Analysis of data for these studies has revealed 2 features. First, the IVD wedge angle changes significantly from cranial to caudal throughout the cervical vertebrae of humans.[17] This is in contrast to the IVD wedge angle of dogs, which is similar among the various segments.[22] Second, the mean IVD wedge angle in humans (7.26°) and dogs (5.0°) can be considered to be similar. However, a fact evident from the data is that the end plates in both species are not oriented parallel to each other.

Measurements of the IVD width were used to determine a 3-D shape of the cervical IVD space of dogs. On the basis of these 3-D shapes, it appeared that the cervical IVD was a semimobile structure, with the central part having an unchanging IVD width, whereas the dorsal and ventral portions of the disk changed significantly throughout motion. Interestingly, the unchanging part was in the location of the nucleus pulposus (a gel-like structure), whereas the changing parts more likely represented the anatomic structure of the annulus fibrosus (a more rigid structure). Although it was not investigated in the study reported

here, we believe that the nucleus pulposus was located in the central concavity, as described within the convex double apices shape. Additionally, the annulus is located in the peripheral part of the end plate (referred to as the epiphyseal rim in humans), which is the convex part of the end plate.[10] The apex described in humans most likely represents the border between the annulus fibrosis and nucleus pulposus.

Considering the difference in shapes between the end plates of humans and dogs, a human prosthesis seems inappropriate for the cervical vertebrae of dogs. Mismatches between prosthesis and end plate shape or IVD wedge angle might also be a causative factor for the clinical complications associated with disk replacement in human spinal surgery.[23,24] An overall complication rate of 26% has been reported, with 3.8% reported as prosthesis migration, which is the main reason for revision surgery[25]; however, long-term evidence is missing. Some human disk prostheses compensate for these mismatches (eg, a built-in lordotic angle[h]), but the biomechanical or clinical advantages of this adaptation have not been scientifically evaluated. Another finding of the present study (ie, the dynamic nature of IVD wedge angles) has been investigated only in humans in the lumbar vertebrae and only in flexion, so it is difficult to make comparisons between the 2 species. In 1 report,[26] a significant variation in the L7-S1 segment of humans was found, with a change in IVD wedge angle during flexion and extension of approximately 40° in the lumbar vertebrae. Because of this variation, it remains speculative whether it will be possible to develop a single IVD prosthesis that compensates for the dynamic movements and prevents implant dislocation or lack of integration.[18]

The design of a prosthesis with regard to its size relative to an end plate remains unclear. The contact area of the only commercially available canine cervical disk prosthesis[i] has not been evaluated, but it seems relatively small, compared with the surface area of a cervical end plate. On the basis of results for the study reported here, it appeared that a prosthesis covering only the central part of the end plates would not need to adapt to the dynamic changes in the periphery of the end plate because the central part of the disk appeared to be static. However, the downside of an implant covering a relatively small end plate surface is an increased risk of subsidence.[23] On the other hand, a prosthesis that also covers the end plate periphery and thus the dynamic areas of the IVD space would need characteristics that would enable the prosthesis to adapt to changing dimensions and a dynamic environment. Hence, finding a material that is capable of compensating for these adaptations in flexibility, size, and shape while remaining attached to the end plates and that does not increase the risk of dislodgment will be a big challenge in the process of developing a cervical IVD prosthesis for dogs. However, the findings for the present study were for healthy grade I IVDs. In contrast, a degenerated disk might not be able to compensate and maintain a static central area (ie, the central part of a degenerated disk might well become dynamic in a manner similar to that of the peripheral area).

The present study had several limitations. First, 2-D measurements were used to describe a 3-D structure, which may have led to inaccurate measurements of disk spaces. By standardizing the orientation of the images through the use of identified landmarks, inaccuracies were limited as much as possible. It was our intent to attain a 3-D description and better understanding of disk spaces and end plates; thus, 3-D modeling would be a valuable next step. Second, the study involved a homogeneous sample population consisting of 5 medium-sized dogs. The animals chosen represented the size of dogs typically affected by disk-associated CSM with IVDs that did not involve degeneration. The same morphometric measurements of degenerated IVDs would be of considerable value, especially when considering the design of a prosthesis for CSM patients.[27] However, it should be mentioned that the role of the static IVD width has been controversial when dogs with and without clinical signs of CSM were compared.[12,13] A comparison of the morphometric dimensions between a healthy and degenerated caudal cervical IVD space is a necessary step for future study.

Also, the cranial and caudal end plates differed in size. Because the IVD width was measured perpendicular to the end plates, this meant that part of the IVD width (the ventral annulus fibrosus) was not measured. However, because an IVD prosthesis will be anchored between 2 adjacent end plates and its cranial and caudal length might be corresponding, this appeared to be the relevant area of the end plate. The longer, ventral tip of a caudal end plate might be less important for an IVD prosthesis design.

Third, although the dorsoventral IVD wedge angle was measured, laterolateral IVD wedge angles were not measured in the present study. On the basis of results of an unpublished experiment performed by our research group in which we found ventral expulsion of a human prosthesis[j] in flexion-extension, the dorsoventral IVD wedge angle was considered the angle of primary interest. A ventral approach is typically performed when inserting a cervical IVD prosthesis, which leaves the lateral borders of the IVD intact. Therefore, it was deemed that the risk of lateral dislocation would be relatively small; thus, the laterolateral angle was not measured in the present study.

Finally, as for all ex vivo studies, the testing setup used in the present study did not allow for true physiologic motion. The vertebrae were moved in a constrained manner that neglected axial loads, torsion, and coupled motions.[28,29] The reason was that for the present study, the predefined end plate landmarks would increase in distance when applying torsion without necessarily causing an increase in IVD width. Therefore, these measurements would not represent a true increase in IVD space. An additional limita-

tion of the ex vivo setup involved the fact that a handheld loading scale was used for applying the desired torque of 1.5 N•m. However, because the angle of the pin in relation to the specimen changed as load was applied, the torque applied was not always 1.5 N•m and differed among specimens. Despite this inaccuracy, we believed that the relative changes in the measured dynamic variables were of value for the designed research because the applied torque was similar among samples and loading positions.

In the study reported here, the caudal cervical IVD spaces of dogs were characterized as semimobile. The dorsal and ventral aspects had changes in size, whereas the center remained unchanged. Furthermore, the caudal cervical IVD spaces and end plates had unique dimensions and dynamic characteristics, which were similar for the 3 most caudal cervical IVD spaces. These findings indicated the complexity of IVD spaces and should be considered when designing IVD prostheses for dogs.

Acknowledgments

This manuscript represents a portion of a thesis submitted by Dr. Knell to the Graduate School for Cellular and Biomedical Sciences, University of Bern, as partial fulfillment of the requirements for a Doctor of Philosophy degree.

Supported in part by the Small Animal Foundation of the University of Zurich.

Presented in abstract form at the 26th Annual Scientific Meeting of the European College of Veterinary Surgeons, Edinburgh, July 2017, and the 1st International Symposium of the Societa Culturale Italiana Veterinari per Animali da Campagnia, Bologna, Italy, April 2018; and in poster form at the 45th Annual Meeting of the Veterinary Orthopedic Society, Snowmass, Colo, March 2018.

The authors thank Jeanne Peter for technical assistance.

Footnotes

a. Adamo PF, da Costa RC, Kroll R, et al. Cervical disc arthroplasty using the Adamo Spinal Disc in 18 dogs affected by disc associated wobbler syndrome (abstr). *J Vet Intern Med* 2013;27:677.
b. Zindl C, Adamo PF, da Costa RC, et al. Retrieval analysis of canine cervical total disc replacement implants (abstr). *Vet Surg* 2015;44:E27.
c. Kirschner-Ehmer apparatus, DePuy Synthes, Oberdorf, Switzerland.
d. Brilliance CT 16-slice machine, Philips AG, Zurich, Switzerland.
e. OsiriX imaging software, version 4.1, 64-bit, Geneva, Switzerland.
f. Program R, R Foundation for Statistical Computing, Vienna, Austria.
g. Graphpad Prism, version 6, Graphpad Software Inc, La Jolla, Calif.
h. DISCOVER, DePuy Synthes, Raynham, Mass.
i. Adamo Spinal Disc, Applied Veterinary Technology, Walnut Creek, Calif.
j. ActiveC, Aesculap, Tuttlingen, Germany.

References

1. Seim HB, Withrow SJ. Pathophysiology and diagnosis of caudal cervical spondylomyelopathy with emphasis on the Doberman Pinscher. *J Am Anim Hosp Assoc* 1982;18:241–251.
2. da Costa RC. Cervical spondylomyelopathy (wobbler syndrome) in dogs. *Vet Clin North Am Small Anim Pract* 2010;40:881–913.
3. da Costa RC, Parent JM, Holmberg DL, et al. Outcome of medical and surgical treatment in dogs with cervical spondylomyelopathy: 104 cases (1988–2004). *J Am Vet Med Assoc* 2008;233:1284–1290.
4. Steffen F, Voss K, Morgan JP. Distraction-fusion for caudal cervical spondylomyelopathy using an intervertebral cage and locking plates in 14 dogs. *Vet Surg* 2011;40:743–752.
5. da Costa RC, Parent JM. One-year clinical and magnetic resonance imaging follow-up of Doberman Pinschers with cervical spondylomyelopathy treated medically or surgically. *J Am Vet Med Assoc* 2007;231:243–250.
6. Jeffery ND, McKee WM. Surgery for disc-associated wobbler syndrome in the dog—an examination of the controversy. *J Small Anim Pract* 2001;42:574–581.
7. Adamo PF. Cervical arthroplasty in two dogs with disk-associated cervical spondylomyelopathy. *J Am Vet Med Assoc* 2011;239:808–817.
8. Adamo PF, Forterre F. Will there be a role for disc prostheses in small animals? In: Fingeroth JM, Thomas WB, eds. *Advances in intervertebral disc disease in dogs and cats.* Ames, Iowa: Willey-Blackwell, 2014;294–309.
9. Ramos RM, da Costa RC, Oliveira ALA, et al. Effects of flexion and extension on the diameter of the caudal cervical vertebral canal in dogs. *Vet Surg* 2015;44:459–466.
10. Wang Y, Battié MC, Videman T. A morphological study of lumbar vertebral endplates: radiographic, visual and digital measurements. *Eur Spine J* 2012;21:2316–2323.
11. Bergknut N, Grinwis G, Pickee E, et al. Reliability of macroscopic grading of intervertebral disk degeneration in dogs by use of the Thompson system and comparison with low-field magnetic resonance imaging findings. *Am J Vet Res* 2011;72:899–904.
12. da Costa RC, Parent JM, Partlow G, et al. Morphologic and morphometric magnetic resonance imaging features of Doberman Pinschers with and without clinical signs of cervical spondylomyelopathy. *Am J Vet Res* 2006;67:1601–1612.
13. De Decker S, Gielen IMVL, Duchateau L, et al. Intervertebral disk width in dogs with and without clinical signs of disk associated cervical spondylomyelopathy. *BMC Vet Res* 2012;8:126–132.
14. Wilke HJ, Geppert J, Kienle A. Biomechanical in vitro evaluation of the complete porcine spine in comparison with data of the human spine. *Eur Spine J* 2011;20:1859–1868.
15. Sheng S-R, Wang X-Y, Xu H-Z, et al. Anatomy of large animal spines and its comparison to the human spine: a systematic review. *Eur Spine J* 2010;19:46–56.
16. Sheng S-R, Xu H-Z, Wang Y-L, et al. Comparison of cervical spine anatomy in calves, pigs and humans. *PLoS One* 2016;11:e0148610.
17. Zhao S, Hao D, Jiang Y, et al. Morphological studies of cartilage endplates in subaxial cervical region. *Eur Spine J* 2016;25:2218–2222.
18. Eijkelkamp MF, Van Donkelaar CC, Veldhuizen AG, et al. Requirements for an artificial intervertebral disc. *Int J Artif Organs* 2001;24:311–321.
19. Lakshmanan P, Purushothaman B, Dvorak V, et al. Sagittal endplate morphology of the lower lumbar spine. *Eur Spine J* 2012;21(suppl 2):S160–S164.
20. van der Houwen EB, Baron P, Veldhuizen AG, et al. Geometry of the intervertebral volume and vertebral endplates of the human spine. *Ann Biomed Eng* 2010;38:33–40.
21. Tang R, Gungor C, Sesek RF, et al. Morphometry of the lower lumbar intervertebral discs and endplates: comparative analyses of new MRI data with previous findings. *Eur Spine J* 2016;25:4116–4131.
22. Gilad I, Nissan M. Sagittal radiographic measurements of the cervical and lumbar vertebrae in normal adults. *Br J Radiol* 1985;58:1031–1034.
23. Thaler M, Hartmann S, Gstöttner M, et al. Footprint mismatch in total cervical disc arthroplasty. *Eur Spine J* 2013;22:759–765.
24. Dong L, Tan M-S, Yan Q-H, et al. Footprint mismatch of cervical disc prostheses with Chinese cervical anatomic dimensions. *Chin Med J (Engl)* 2015;128:197–202.

25. Wu T-K, Liu H, Ning N, et al. Cervical disc arthroplasty for the treatment of adjacent segment disease: a systematic review of clinical evidence. *Clin Neurol Neurosurg* 2017;162:1–11.
26. Chen M-W, Yang S-W, Lee M-C. Changes in lumbar disc angles of Chinese subjects from upright to flexion. *Spine* 1994;19:1490–1494.
27. Tibrewal SB, Pearcy MJ. Lumbar intervertebral disc heights in normal subjects and patients with disc herniation. *Spine* 1985;10:452–454.
28. Johnson JA, da Costa RC, Bhattacharya S, et al. Kinematic motion patterns of the cranial and caudal canine cervical spine. *Vet Surg* 2011;40:720–727.
29. Hofstetter M, Gédet P, Doherr M, et al. Biomechanical analysis of the three-dimensional motion pattern of the canine cervical spine segment C4–C5. *Vet Surg* 2009;38:49–58.